Nuclear dissipation and isospin relaxation in ^{20}Ne + ^{116,124}Sn reactions

Payel Karmakar,[1,2] Samir Kundu,[1,2,*] T. K. Rana,[1,2] S. Manna,[1,2] R. Pandey,[1] C. Bhattacharya,[1,2] K. Banerjee,[1,2] Pratap Roy,[1,2] Arijit Sen,[1,2] T. K. Ghosh,[1,2] G. Mukherjee,[1,2] S. Mukhopadhyay,[1,2] D. Paul,[1,2] M. Shaikh,[1] S. Nandi,[1,2,†] and S. Dalal[1]

[1]*Variable Energy Cyclotron Centre, 1/AF Bidhan Nagar, Kolkata 700064, India*

[2]*Homi Bhabha National Institute, Training School Complex, Anushakti Nagar, Mumbai 400094, India*

(Received 16 January 2024; revised 30 April 2024; accepted 21 May 2024; published 8 July 2024)

Inclusive energy distributions of isotopically resolved intermediate-mass fragments with $Z = 3$–6 have been measured for the reactions ^{20}Ne + ^{116}Sn and ^{20}Ne + ^{124}Sn at two excitation energies, 0.86 and 1.06 MeV/nucleon. The peak of energy spectra of each fragment is much higher than the peaks expected from asymmetric fission. The angular distributions of all fragments fall much faster than $\frac{1}{\sin\theta_{\mathrm{c.m.}}}$ which shows that fragments are emitted from a nonequilibrated source, produced in a highly energy-damped deep-inelastic collision. The lifetimes of the dinuclear composites extracted from the angular distribution of different fragments were found in the range of $\approx(0.5-3)\times10^{-22}$ s. Angular momentum dissipation factors have been extracted for each of the emitted isotopes. The mean angular momentum dissipation factor nearly matches with sticking limit predictions for the lighter fragments but gradually increases with the increase of fragment mass relative to the sticking limit predictions in both the reactions. In this study it is found that the neutron-rich system ^{20}Ne + ^{124}Sn tends to emit neutron-rich isotopes, whereas the neutron-deficient system ^{20}Ne + ^{116}Sn favors the emission of neutron-deficient isotopes at both energies, suggesting isospin relaxation. However, the variation in isotopic yield ratios with kinetic energy for certain isotopes indicates that isospin relaxation is incomplete at the higher excitation energy of 1.06 MeV/nucleon.

DOI: 10.1103/PhysRevC.110.014608

I. INTRODUCTION

The emission mechanism of intermediate-mass fragments (IMFs) released in heavy-ion reactions is an interesting topic, and many theoretical [1–6] and experimental [7–24] studies have been done in the energy range of $\lesssim$15 MeV/nucleon. All these studies have shown that IMFs are emitted mainly due to fusion-fission, deep-inelastic collisions, incomplete fusion, deep-inelastic orbiting, quasielastic scattering, etc. At lower energy, fully energy dissipated mechanisms, like fusion-fission dominate, whereas at higher energy, well above the Coulomb barriers, partially energy-dissipated mechanisms like deep-inelastic collisions (DICs) are increasingly dominating. As DIC is an indeterminate process between quasielastic and complete fusion [25], it is used as an important probe to study the several complex dynamical features of nuclear interaction like nucleon transport, energy dissipation, and angular momentum dissipation. The DIC is greatly influenced by the beam energy of the projectile, the relative angular momentum, the mass asymmetry, and the charge product of colliding nuclei. With the increase of all these parameters, the contribution of the DIC increases with respect to the fusion-fission process [26]. A large fraction of the kinetic energy of relative motion is transformed as the intrinsic excitation energy of both the emitted fragments. Also, the relative angular momentum is transformed as the intrinsic spin of both the emitted fragments. During a collision, both the colliding nuclei exchange charge and mass [27].

Many studies have been done on DIC and relaxation of different degrees of freedom using IMF emission. However, measurement of isotopic mass and energy distributions of the emitted IMF from the systems having different N/Z are scarce [28], particularly in mid-heavy systems like those in the present study. An advanced detector system allows us to study DIC collision by measuring isotopic mass and energy distributions of the emitted IMF. In this paper, we shall report our study on nuclear dissipation and relaxation of isospin degrees of freedom in ^{20}Ne + ^{116,124}Sn systems having different N/Z ratios at two different excitation energies, 0.86 and 1.06 MeV/nucleon. N/Z ratios of the produced composites, ^{136}Nd and ^{144}Nd, are 1.27 and 1.40, respectively.

The article is arranged as follows. Experimental details are described in Sec. II, results are presented in Sec. III, and discussion on the experimental results is in Sec. IV. Finally, the conclusions are given in Sec. V.

II. EXPERIMENTAL DETAILS

The experiment was performed using an accelerated neon-ion beam from the K130 cyclotron at VECC, Kolkata. The fragments emitted from the reactions ^{20}Ne (160 and 192 MeV) + ^{116}Sn and ^{20}Ne (157.4, 192 MeV) + ^{124}Sn were detected isotopically using a $\Delta E - E$ detector telescope. It covered an angular range of $\approx$20°–35° in the laboratory. The ΔE detector

*Contact author: skundu@vecc.gov.in

†Present address: Subatech (IMT Atlantique, CNRS/IN2P3, Nantes Université) 4 rue Alfred Kastler 44307, Nantes cedex 3, France.

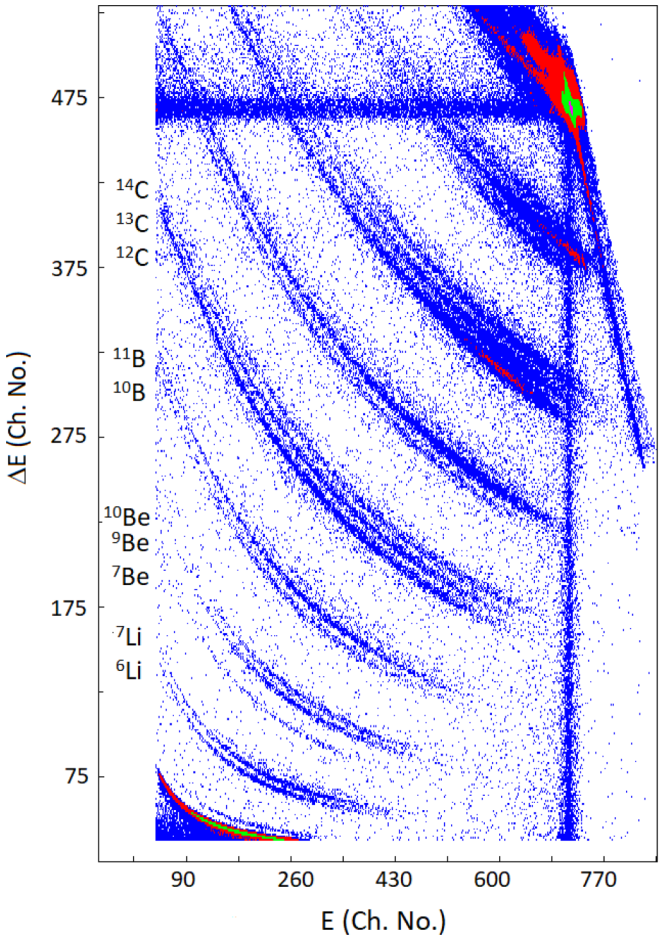

FIG. 1. Typical 2D energy spectrum of IMFs obtained in the reaction ^{20}Ne (192 MeV) + ^{124}Sn using a $\Delta E - E$ charged particle telescope.

consists of a silicon strip detector with a thickness ≈50 μm, with 16 vertical strips on its front side. The E detector has a thickness of ≈1034 μm with 16 vertical strips in the front side and 16 horizontal strips in the back side. The width of each strip is 3 mm. In the front of the telescope, a slit of 8 mm in height and 52 mm in width was used to restrict the detection of the scattered particles only in the reaction plane. The center of the telescope was kept at a distance of 195 mm from the target. The solid angle covered by the central strip was 0.63 mSr. A typical two-dimensional (2D) energy spectrum of IMFs obtained in the reaction ^{20}Ne (192 MeV) + ^{124}Sn at $\theta_{\rm lab} \approx 21^\circ$ is shown in Fig. 1. It is seen that all the bands for the isotopes ^{6}Li, ^{7}Li, ^{7}Be, ^{9}Be, ^{10}Be, ^{10}B, ^{11}B, ^{12}C, ^{13}C, and ^{14}C are clearly separated. The calibration of the telescope was done using a ^{229}Th α-source and elastically scattered neon from tin and gold targets. The thickness and purity of the ^{116,124}Sn targets are ≈378 and 406 μg/cm^2 and ≈98% and ≈99.9%, respectively.

III. RESULTS

A. Energy spectra

Typical energy spectra of the different isotopes of various fragments obtained in ^{20}Ne (192 MeV) + ^{116}Sn and ^{20}Ne (192 MeV) + ^{124}Sn reactions are shown in Figs. 2 and 3, respectively. The spectra are typically Gaussian in shape. The lower part of the energy spectra of heavier fragments is truncated because of the finite thickness of the ΔE detector. However, this does not adversely affect our analysis since we are interested in the nonequilibrium part of the spectra. A Gaussian was fitted with each experimental spectrum using the higher-energy part of the same, as shown by the green line in Figs. 2 and 3, to extrapolate the lower-energy part of the spectra. The blue arrows indicate the most probable energy if a fully energy-equilibrated compound nucleus emits the fragments by asymmetric fission. These are calculated assuming binary fission of the ^{136}Nd and ^{144}Nd with total energy obtained from Viola systematics [29] corrected by the asymmetric factor $4Z_1Z_2/(Z_1+Z_2)^2$ [30]. These arrows were observed to lie at the lower part of the energy spectra of each fragment. This indicates that the fragments are emitted from a nonequilibrated source. Similar energy spectra were observed for the reactions at the excitation energy of 0.86 MeV/nucleon.

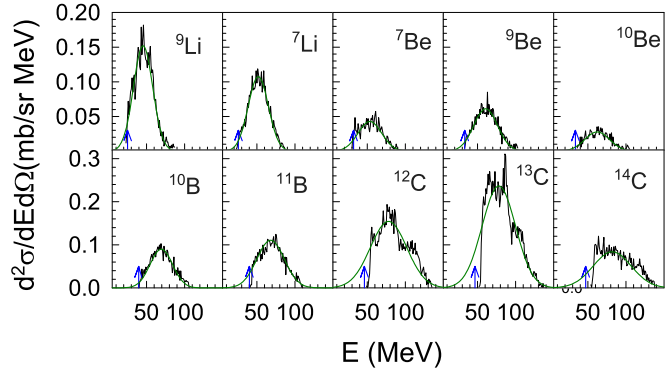

FIG. 2. Typical energy spectra of different isotopes of Li, Be, B, and C obtained in the reaction ^{20}Ne (192 MeV) + ^{116}Sn at $\theta_{\rm lab} \approx 26.5^\circ$. The green solid lines represent the Gaussian fitted with the higher-energy part of the experimental spectra. Arrows indicate the average kinetic energies of the corresponding isotopes obtained from the Viola systematics corrected by the corresponding asymmetric factors [30].

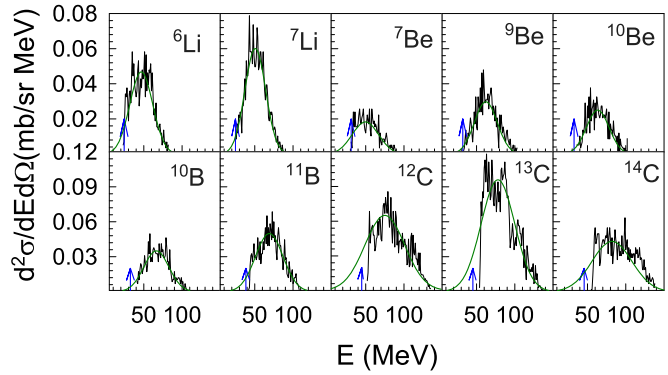

FIG. 3. Same as Fig. 2 but for the reaction ^{20}Ne (192 MeV) + ^{124}Sn.

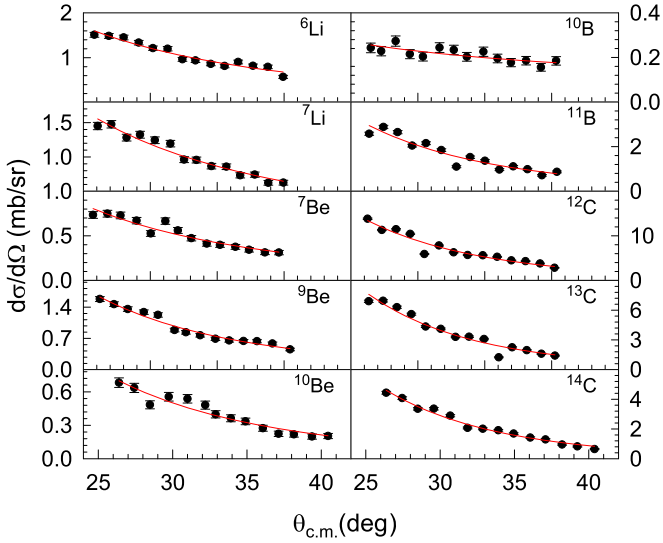

FIG. 4. Solid circles show the angular distribution of different fragments emitted from the reaction ^{20}Ne (160 MeV) + ^{116}Sn. Red lines were obtained by fitting the experimental data with Eq. (1).

B. Angular distributions

The angular distributions were obtained by integrating the different Gaussians fitted with experimental energy spectra obtained at different angles in the range of 20°–35°. The cross section ($d\sigma/d\Omega$) was converted to the center of mass (c.m.) frame by assuming two-body kinematics averaged over total kinetic energy distributions. Angular distributions of different fragments emitted from different reactions ^{20}Ne (160 MeV) + ^{116}Sn, ^{20}Ne (157.4 MeV) + ^{124}Sn, ^{20}Ne (192 MeV) + ^{116}Sn, and ^{20}Ne (192 MeV) + ^{124}Sn are shown in Figs. 4–7, respectively. It was found that the angular distributions fall much faster than $\frac{1}{\sin\theta_{\text{c.m.}}}$, which indicates that fragments are emitted from nonequilibrated sources having shorter lifetimes. The lifetime τ_{DI} of the composite can be calculated using a diffractive Regge-pole model [11]. The angular distributions of the fragments were fitted well with the equation

$$d\sigma/d\Omega \propto \frac{1}{\sin\theta_{\text{c.m.}}} e^{-\frac{\theta_{\text{c.m.}}}{\omega\tau_{\text{DI}}}}, \tag{1}$$

where $\omega = \frac{\hbar L}{\mu d^2}$ is the angular velocity of the rotating dinucleus, μ is the reduced mass of the system, d represents the distance between the two centers of the dinucleus, and $\theta_{\text{c.m.}}$ is the scattering angle in the center of mass (c.m.) frame. The red lines in the figures were obtained by fitting the experimental data with the above equation. Good fitting indicates that fragments might be emitted from deep-inelastic (DI) collisions.

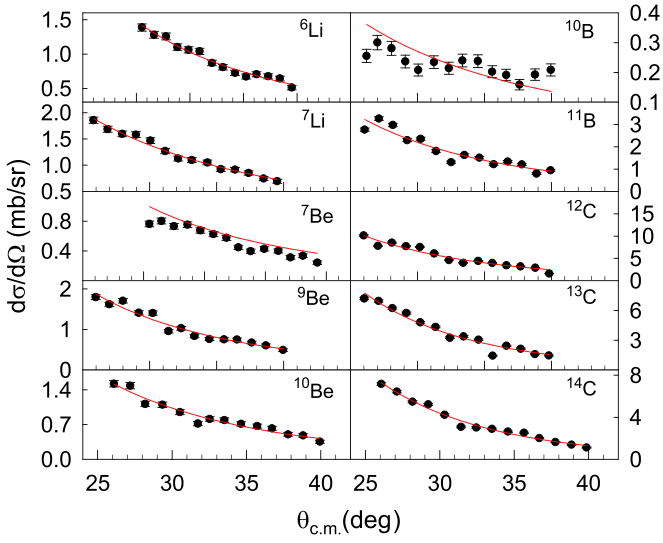

FIG. 5. Same as Fig. 4 but for the reaction ^{20}Ne (157.4 MeV) + ^{124}Sn.

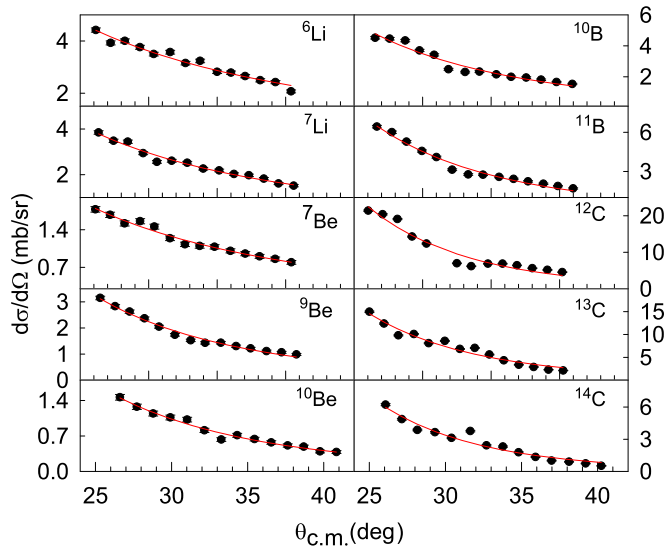

FIG. 6. Same as Fig. 4 but for the reaction ^{20}Ne (192 MeV) + ^{116}Sn.

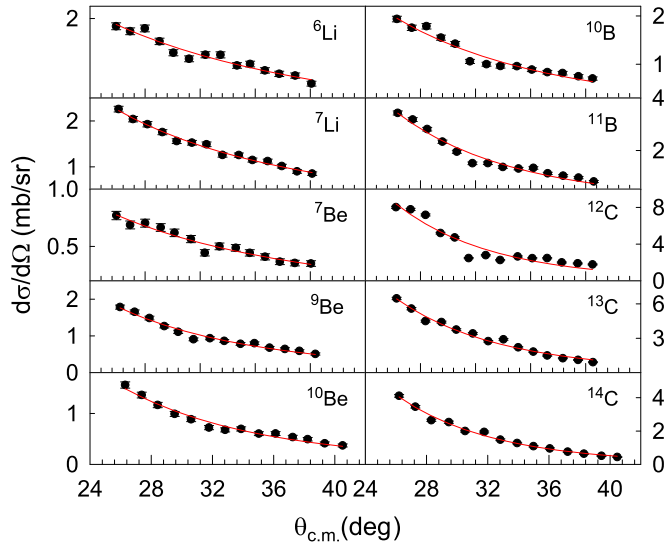

FIG. 7. Same as Fig. 4 but for the reaction ^{20}Ne (192 MeV) + ^{124}Sn.

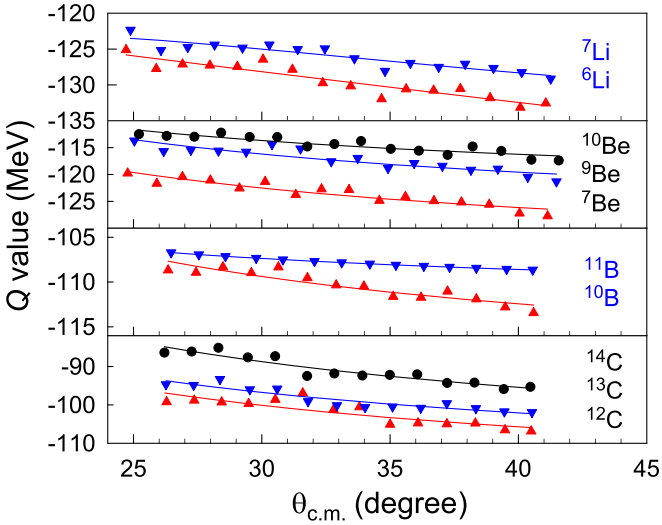

FIG. 8. Q value distribution of different isotopes emitted in the reaction ^{20}Ne (192 MeV) + ^{124}Sn. Solid lines are there to guide the eye.

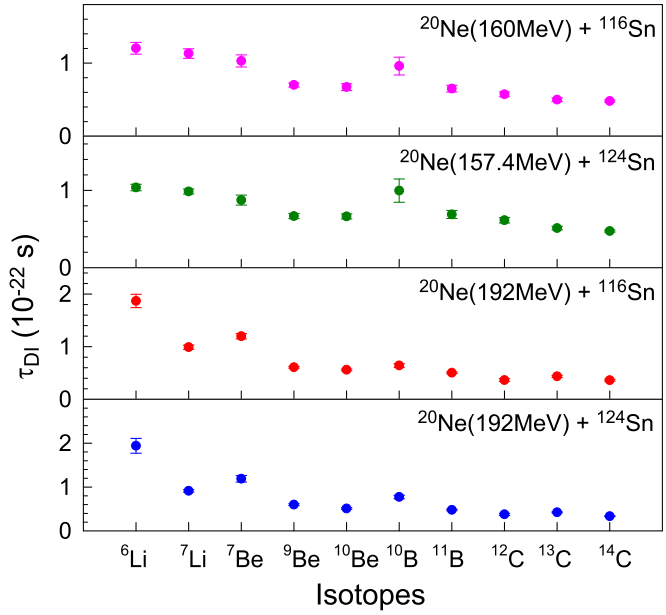

FIG. 9. Emission timescale of different DI fragments.

C. Q value distributions

The Q value of the reaction for each fragment has been extracted from the average kinetic energy of the fragments using two-body kinematics. It has been observed that the Q value decreases with the increase of scattering angle for fragments under the present study in all reactions. Typical Q value distributions of different isotopes emitted in the reaction ^{20}Ne (192 MeV) + ^{124}Sn are shown in Fig. 8. This figure shows that with the increase of angle, the Q value decreases, indicating that the systems move towards more equilibrium. All the other reactions follow the same trend.

D. The timescale of the emission

The timescale ($\tau_{\rm DI}$) of the emission was extracted by fitting Eq. (1) with the angular distribution of the measured differential cross section. This fitting gives the value of the parameter $\omega\tau_{\rm DI}$ as mentioned above. The angular velocity of the rotating dinucleus, $\omega = \frac{\hbar L}{\mu d^2}$, depends on the dinuclear separation d and the angular momentum L. It is observed above that the Q value is more negative at a larger angle. This shows that the energy dissipation is more at a larger angle, and the system moves towards complete energy damping like the compound nucleus (CN). This corresponds to more compact dinuclear systems like the scission shape of a fissioning CN. For such a shape, d and L of the DIC will be similar to the scissioning CN. d is the center-to-center distance between the two emitted fragments, and L is taken as $L_{\rm cr}$ for fusion and calculated using the Bass model [31]. Another extreme of DIC is the grazing collision, for which fragments will be emitted at the most forward angle. In this case, L should be considered as $L_{\rm gr}$ and d is to be taken as the center-to-center distance between two colliding nuclei, the target and the projectile.

The emission timescale of different DI fragments emitted in different reactions is plotted in Fig. 9 for $L = L_{\rm cr}$. It has been found that the emission timescale decreases with the increase of mass of the fragments for all reactions. It is expected that the lighter fragments would need more nucleon exchange and, hence, more time. The range of the timescale is $\approx(0.5 - 3) \times 10^{-22}$ s.

E. Angular momentum dissipation

The study of angular momentum dissipation is important to understand the energy-damping mechanism in deep inelastic collisions. Like energy, relative angular momentum is also partially dissipated as the internal spin of the emitted fragments. Nondissipated angular momentum adds extra energy as rotational kinetic energy to the emitted fragments over the contribution from Coulomb and nuclear forces. The total kinetic energy of the rotating dinuclear system, E_k, is given by

$$E_k = V_N(d) + f^2 \frac{\hbar^2 L_i(L_i+1)}{2\mu d^2}, \qquad (2)$$

where $V_N(d)$ is the contribution of Coulomb and nuclear forces at the separation distance d of the rotating dinuclear system at its scission shape, i.e., center-to-center distance of the two emitting fragments, μ is the reduced mass of the dinuclear system, L_i is the relative angular momentum in the entrance channel, and f is the angular momentum dissipation factor, which denotes the ratio of the final angular momentum, L_f, to the initial angular momentum, L_i. A simple prescription was given to extract f in Ref. [32]. There, it was found that angular momentum dissipation factor for the fully energy-damped DI collision is close to the corresponding rigid rotation limit (sticking limit) in the case of few light systems. To check whether the same trend persists for the present systems, the angular momentum dissipation factors have been extracted for all the detected isotopes.

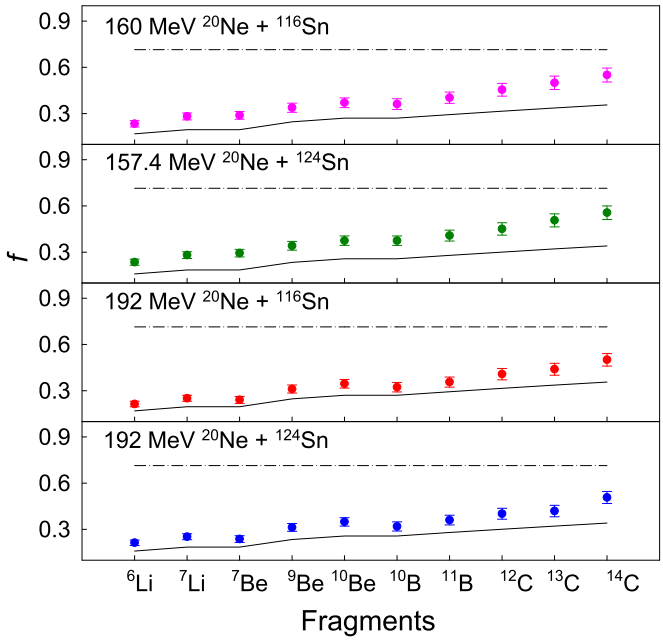

FIG. 10. Variations of angular momentum dissipation factor f with DI fragments. The solid lines and dashed-dot-dashed lines represent the sticking and rolling limit predictions, respectively.

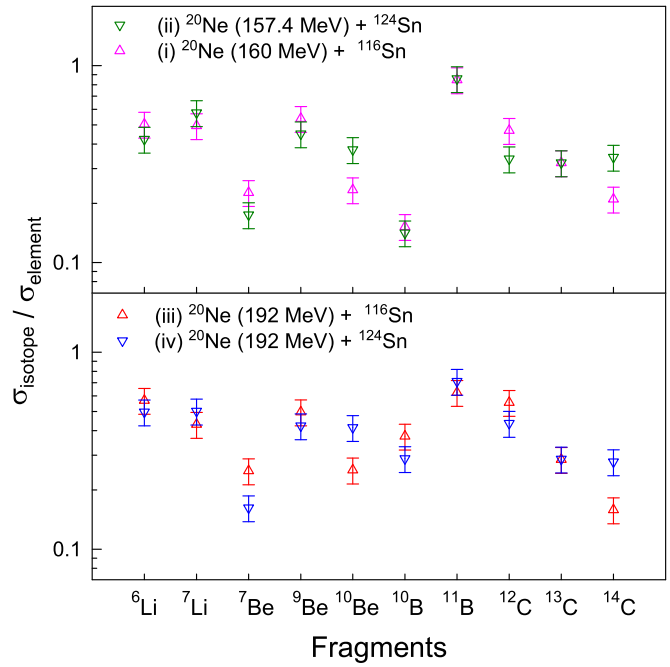

FIG. 11. Ratio of isotopic cross sections to their total elemental cross sections of different isotopes emitted in reactions as indicated in the figure.

As it is discussed above, DIC takes place in the range of angular momentum $L_{cr} \lesssim L \lesssim L_{gr}$. The fusion-fission is most dominated around L_{cr}. So, the scission shape of the dinuclear composite, as in the case of fusion-fission, may be considered to calculate d for the fully energy-damped DI yields [8]. The dinuclear separation d is calculated from the center-to-center distance between the two emitted binary fragments in touching conditions. This d is used to extract the value of f, and L_i is taken as L_{cr} [31]. The value of d varies between ≈7.8 and 8.4 fm for all the fragments from ^{6}Li to ^{14}C, respectively, emitted in binary reactions. The values of L_{cr} are 70$\hbar$ and 72$\hbar$ for ^{20}Ne + ^{116}Sn at the beam energies of 160 and 192 MeV, respectively, and 80$\hbar$ and 83$\hbar$ for the ^{20}Ne + ^{124}Sn reaction at 157.4 and 192 MeV, respectively. Using these values of d and L_i, the mean angular momentum dissipation factor f has been extracted for all the fragments emitted in the reactions under the present study and plotted in Fig. 10.

F. Dependence of cross sections on target N/Z

The total cross sections of all fragments have been extracted by integrating Eq. (1). The ratio of the isotopic cross sections to the total elemental cross sections of different isotopes emitted in the reactions (i) ^{20}Ne(160 MeV) + ^{116}Sn, (ii) ^{20}Ne(157.4 MeV) + ^{124}Sn, (iii) ^{20}Ne(192 MeV) + ^{116}Sn, and (iv) ^{20}Ne(192 MeV) + ^{124}Sn are plotted in Fig. 11. It is observed that the yield of the most neutron-rich isotope of a particular fragment is higher in the case of the reaction involving the neutron-rich nuclei, and the yield of the most neutron-deficient isotope is higher in the neutron-deficient composite. For example, the yields of the relatively neutron-deficient ^{6}Li, ^{7}Be, etc., are more in the ^{20}Ne + ^{116}Sn system, whereas the yields of the relatively neutron-rich isotopes ^{7}Li, ^{10}Be, and ^{14}C are more in the ^{20}Ne + ^{124}Sn system. This trend is followed at both the energies.

G. Isotopic yield ratio at different kinetic energy

As we saw in Sec. III D, the emission timescale of IMFs is in the range of ≈$(0.5 - 3) \times 10^{-22}$ s. If the timescale is shorter than the equilibration time, then emitted fragments may retain the N/Z of the projectile and/or the target. The projectilelike fragments emitted in the DICs are slowed down because of strong energy dissipation. In such kinds of reactions, the velocity of the emitted fragments is a good physical quantity to compare the emission time, which is proportional to the square root of the kinetic energy in MeV/nucleon [33]. In Figs. 12 and 13, ratios of the yield of the different isotopes have been plotted at their different kinetic energies. It is observed in Fig. 12 that the ratio of the isotopes are nearly constant within error bars at all kinetic energy for reactions (i) ^{20}Ne (160 MeV) + ^{116}Sn and (ii) ^{20}Ne (157.4 MeV) + ^{124}Sn, whereas in Fig. 13, only ^{6}Li / ^{7}Li, ^{10}Be / ^{9}Be, and ^{14}C / ^{13}C are nearly constant within error bars for reactions (iii)^{20}Ne (192 MeV) + ^{116}Sn and (iv) ^{20}Ne (192 MeV) + ^{124}Sn. However, for other elements, ^{7}Be / ^{9}Be and ^{12}C / ^{13}C, the ratio is increasing above kinetic energy ≈8 MeV/nucleon. In the case of ^{10}B / ^{11}B, the ratio is increasing from the lowest to the highest measured energy.

IV. DISCUSSION

The energy distributions, angular distributions, Q value distributions, and emission timescale show that all the fragments emitted in all the reactions under the present study

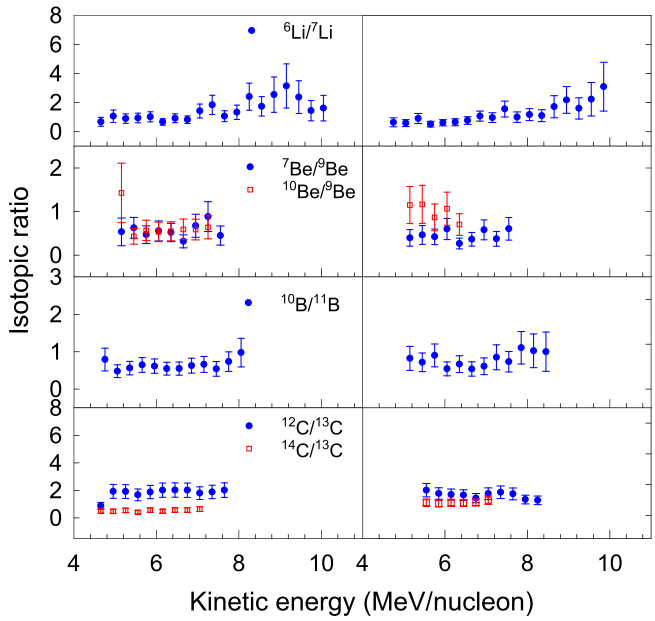

FIG. 12. The ratio of yields of isotopes Li, Be, B, and C, measured at 26.5°, emitted in reactions (i)^{20}Ne (160 MeV) + ^{116}Sn (left panels) and (ii) ^{20}Ne (157.4 MeV) + ^{124}Sn (right panels).

are originated primarily from the DI collisions. The absence or lower yield of the IMFs under the present study around the energy obtained by Viola systematics can be explained as follows. The fissility parameters x of the excited composites, ^{136}Nd and ^{144}Nd, are 0.53 and 0.50, respectively. These are well above the Businaro-Gallone point ($x_{BG} = 0.396$ for $L = 0$ and decreases for larger L values). So, symmetric fission [34] will be dominated by these two systems. The mass of the IMFs in the present study is much less than the fragments emitted in the symmetric fission and the probability of emission of the same by the asymmetric fission will also be lower.

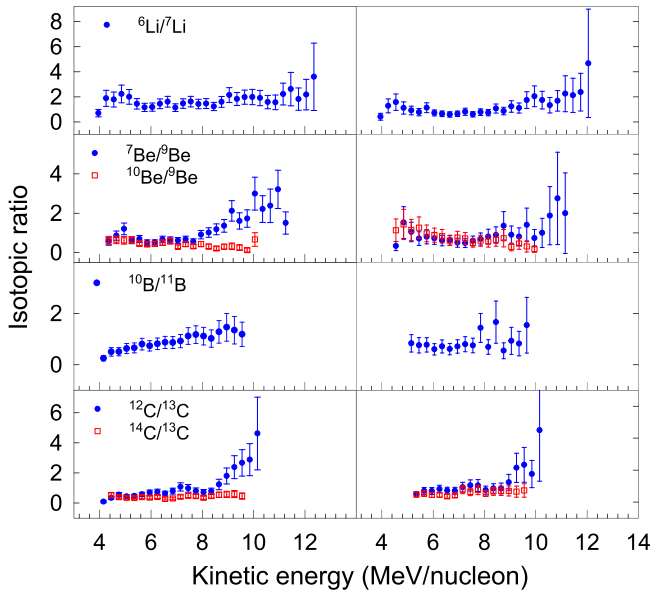

FIG. 13. Same as Fig. 12 but at different beam energy: (iii)^{20}Ne (192 MeV) + ^{116}Sn (left panels) and (iv) ^{20}Ne (192 MeV) + ^{124}Sn (right panels).

The extracted values of angular momentum dissipation factors are compared with the sticking and rolling limit predictions [25]. It was observed that in all the systems, f nearly matches with the sticking limit predictions for the lighter fragments but gradually increases (dissipation decreases) with the increase of fragment mass relative to the sticking limit predictions. This may be explained qualitatively by nuclear friction. Energy or angular momentum dissipation is caused by nuclear friction during the collision because of the exchange of nucleons between the colliding nuclei. This exchange takes place in the overlapping region of the participant nuclei. More friction means more overlap and more nucleon exchange. In the case of lighter fragments, nucleon exchange is more and, hence, the friction increases. These originate from deeper collisions for which the interaction time is also longer. So, the angular momentum dissipation will also be higher in lighter fragments.

The ratio of the isotopic cross section to the total elemental cross section was found to be dependent upon the N/Z of the produced composites. It was found that the neutron-rich system ^{20}Ne + ^{124}Sn favors the emission of neutron-rich isotopes, while the neutron-deficient system ^{20}Ne + ^{116}Sn favors the emission of neutron-deficient isotopes at both energies.

It was observed that the ratio of the yields of all isotopes at lower beam energy and some isotopes at higher energy remain constant as a function of kinetic energy of the fragments. Constant ratios indicate that the isospin degrees of freedom reach equilibration before their emission. The increase of the yield ratio of ^{7}Be / ^{9}Be, ^{10}B / ^{11}B, and ^{12}C / ^{13}C with kinetic energy shows that these fragments are emitted by a dynamic dissipation process, where the isospin is not fully equilibrated at higher beam energy.

V. CONCLUSION

Isotopic yields of the fragments ($3 \leqslant Z \leqslant 6$) emitted from the reactions ^{20}Ne (160 and 192 MeV) + ^{116}Sn and ^{20}Ne (157.4 and 192 MeV) + ^{124}Sn have been studied. The double differential cross sections of the fragments have been measured in the angular range of ≈25°–40° in c.m. The c.m. angular distributions of the fragments follow the equation $d\sigma/d\Omega \propto \frac{1}{\sin\theta_{c.m.}} e^{-\frac{\theta_{c.m.}}{\omega\tau_{DI}}}$. The timescale of the DI process have been extracted from these angular distributions. It has been observed that the timescale gradually decreases as the mass of the emitted fragments increases. The average Q value also decreases with the increase of angle. All these signatures show that the fragments are emitted from deep-inelastic collisions. Assuming a compact scission shape like fusion-fission, angular momentum dissipation factors for all the fragments have been extracted. It was observed that in all the systems, f nearly matches the sticking limit predictions for the lighter fragments but gradually increases (dissipation decreases) with the increase of fragment mass relative to the sticking limit predictions. The greater deviation for heavier fragments may be related to fewer numbers of nucleon exchanges, which

causes less nuclear friction. Cross sections were calculated by integrating the angular distributions of the emitted fragments. The isotopic yield ratio of the fragments was calculated, and it was found that the ratio of the isotopic cross section to the total elemental cross section is dependent upon the N/Z of the colliding nuclei, which is an indication of isospin relaxation. However, variation of isotopic yield ratio with kinetic energy for some of the isotopes shows the incompleteness in isospin relaxation at higher beam energy.

ACKNOWLEDGMENTS

The authors thank Jaikiran Meena, Ruchismita Mondal Saha, Amiya Kumar Saha, and Jayanta Kumar Sahoo for their help during the experiment. We also thank the VECC Cyclotron operators for the smooth running of the accelerator. One of the authors, S.K., would like to thank Sailajanda Bhattacharya for his valuable suggestion on preparing the manuscript.

[1] L. G. Moretto and G. J. Wozniak, Prog. Part. Nucl. Phys. **21**, 401 (1988), and references therein.
[2] R. J. Charity, D. R. Bowman, Z. H. Liu, R. J. McDonald, M. A. McMahan, G. J. Wozniak, L. G. Moretto, S. Bradley, W. L. Kehoe, and A. C. Mignerey, Nucl. Phys. A **476**, 516 (1988).
[3] R. J. Charity, M. A. McMahan, G. J. Wozniak, R. J. McDonald, L. G. Moretto, D. G. Sarantites, L. G. Sobotka, G. Guarino, A. Pantaleo, L. Fiore, A. Gobbi, and K. D. Hildenbrand, Nucl. Phys. A **483**, 371 (1988).
[4] S. A. Kalandarov, G. G. Adamian, N. V. Antonenko, W. Scheid, and J. P. Wieleczko, Phys. Rev. C **84**, 064601 (2011).
[5] A. K. Dhara, C. Bhattacharya, S. Bhattacharya, and K. Krishan, Phys. Rev. C **48**, 1910 (1993).
[6] A. Szanto de Toledo, S. J. Sanders, and C. Beck, Phys. Rev. C **56**, 558 (1997).
[7] T. K. Rana, S. Kundu, C. Bhattacharya, S. Manna, P. Roy, R. Pandey, A. Sen, T. K. Ghosh, G. Mukherjee, K. Banerjee, S. Mukhopadhyaya, D. Paul, M. M. Shaikh, S. Nandi, V. Srivastava, J. K. Sahoo, J. K. Meena, A. K. Saha, R. M. Saha, S. Dalal, and S. Bhattacharya, Phys. Rev. C **103**, 034614 (2021), and references therein.
[8] S. Kundu, C. Bhattacharya, K. Banerjee, T. K. Rana, S. Bhattacharya, A. Dey, T. K. Ghosh, G. Mukherjee, J. K. Meena, P. Mali, S. Mukhopadhyay, D. Pandit, H. Pai, S. R. Banerjee, D. Gupta, P. Banerjee, S. Kumar, A. Shrivastava, A. Chatterjee, K. Ramachandran *et al.*, Phys. Rev. C **85**, 064607 (2012).
[9] L. G. Moretto, Nucl. Phys. A **247**, 211 (1975).
[10] S. J. Sanders, A. Szanto de Toledo, and C. Beck, Phys. Rep. **311**, 487 (1999), and references therein.
[11] C. Beck, R. Nouicer, D. Mahboub, B. Djerroud, R. M. Freeman, A. Hachem, T. Matsuse, S. Cavallaro, E. De Filippo, G. Lanzanó, A. Pagano, M. L. Sperduto, R. Dayras, E. Berthoumieux, R. Legrain, and E. Pollacco, Eur. Phys. J. A **2**, 281 (1998).
[12] G. Ademard, J. P. Wieleczko, J. Gomez del Campo, M. La Commara, E. Bonnet, M. Vigilante, A. Chbihi, J. D. Frankland, E. Rosato, G. Spadaccini, S. A. Kalandarov, C. Beck, S. Barlini, B. Borderie, R. Bougault, R. Dayras, G. De Angelis, J. De Sanctis, V. L. Kravchuk, P. Lautesse *et al.*, Phys. Rev. C **83**, 054619 (2011).
[13] W. U. Schröder and J. R. Huizenga, Annu. Rev. Nucl. Sci. **27**, 465 (1977).
[14] S. Cavallaro, E. De Filippo, G. Lanzanò, A. Pagano, M. L. Sperduto, R. Dayras, R. Legrain, E. Pollacco, C. Beck, B. Djerroud, R. M. Freeman, F. Haas, A. Hachem, B. Heusch, D. Mahboub, A. Morsad, R. Nouicer, and S. J. Sanders, Phys. Rev. C **57**, 731 (1998).
[15] N. Carlin Filho, M. M. Coimbra, N. Added, R. M. dos Anjos, L. Fante, M. C. S. Figueira, V. Guimaraes, E. M. Szanto, A. Szanto de Toledo, and O. Civitarese, Phys. Rev. C **40**, 91 (1989).
[16] S. Szilner, F. Haas, Z. Basrak, R. M. Freeman, A. Morsad, and M. P. Nicoli, Nucl. Phys. A **779**, 21 (2006).
[17] C. Bhattacharya, A. Dey, S. Kundu, K. Banerjee, S. Bhattacharya, S. Mukhopadhyay, D. Gupta, T. Bhattacharjee, S. R. Banerjee, S. Bhattacharyya, T. Rana, S. K. Basu, R. Saha, S. Bhattacharjee, K. Krishan, A. Mukherjee, D. Bandopadhyay, and C. Beck, Phys. Rev. C **72**, 021601(R) (2005).
[18] A. Pop, A. Andronic, I. Berceanu, M. Duma, Moisă, M. Petrovici, V. Simion, A. Bonasera, G. Immé, G. Lanzanò, A. Pagano, G. Raciti, N. Colonna, G. d'Erasmo, A. Pantaleo, H. Feldmeier, and J. Schnack, Nucl. Phys. A **679**, 793 (2001), and references therein.
[19] C. Beck, D. Mahboub, R. Nouicer, T. Matsuse, B. Djerroud, R. M. Freeman, F. Haas, A. Hachem, A. Morsad, M. Youlal, S. J. Sanders, R. Dayras, J. P. Wieleczko, E. Berthoumieux, R. Legrain, E. Pollacco, S. Cavallaro, E. De Filippo, G. Lanzanó, A. Pagano, and M. L. Sperduto, Phys. Rev. C **54**, 227 (1996).
[20] K. A. Farrar, S. J. Sanders, A. K. Dummer, A. T. Hasan, F. W. Prosser, B. B. Back, I. G. Bearden, R. R. Betts, M. P. Carpenter, B. Crowell, M. Freer, D. J. Henderson, R. V. F. Janssens, T. L. Khoo, T. Lauritsen, Y. Liang, D. Nisius, A. H. Wuosmaa, C. Beck, R. M. Freeman *et al.*, Phys. Rev. C **54**, 1249 (1996).
[21] R. M. Anjos, N. Added, N. Carlin, L. Fante, M. C. S. Figueira, R. Matheus, H. R. Schelin, E. M. Szanto, C. Tenreiro, A. Szanto de Toledo, and S. J. Sanders, Phys. Rev. C **48**, R2154 (1993).
[22] D. Shapira, D. Schull, J. L. C. Ford, B. Shivakumar, R. L. Parks, R. A. Cecil, and S. T. Thornton, Phys. Rev. Lett. **53**, 1634 (1984).
[23] W. Dünnweber, A. Glaesner, W. Hering, D. Konnerth, R. Ritzka, W. Trombik, J. Czakański, and W. Zipper, Phys. Rev. Lett. **61**, 927 (1988).
[24] L. G. Sobotka, C. C. Hsu, G. J. Wozniak, G. U. Rattazzi, R. J. McDonald, A. J. Pacheco, and L. G. Moretto, Phys. Rev. Lett. **46**, 887 (1981).
[25] R. Bass, *Nuclear Reactions with Heavy Ions*, 1st ed. (Springer-Verlag, Berlin, 1980).
[26] R. Eggers, M. N. Namboodiri, P. Gonthier, K. Geoffroy, and J. B. Natowitz, Phys. Rev. Lett. **37**, 324 (1976).
[27] D. Agassi, C. Ko, and H. Weidenmüller, Ann. Phys. **107**, 140 (1977).
[28] S. Pirrone, G. Politi, B. Gnoffo, M. La Commara, E. De Filippo, P. Russotto, M. Trimarchi, M. Vigilante, M. Colonna, S. A. Kalandarov *et al.*, Eur. Phys. J. A **55**, 22 (2019).
[29] V. E. Viola, K. Kwiatkowski, and M. Walker, Phys. Rev. C **31**, 1550 (1985).
[30] C. Beck, B. Djerroud, F. Haas, R. M. Freeman, A. Hachem, B. Heusch, A. Morsad, M. Youlal, Y. Abe, A. Dayras, J. P.

Wieleczko, B. T. Matsuse, and S. M. Lee, Z. Phys. A **343**, 309 (1992).
[31] R. Bass, Phys. Rev. Lett. **39**, 265 (1977).
[32] C. Bhattacharya, S. Bhattacharya, T. Bhattacharjee, A. Dey, S. Kundu, S. R. Banerjee, P. Das, S. K. Basu, and K. Krishan, Phys. Rev. C **69**, 024607 (2004).
[33] H.-Y. Wu, Z.-G. Xiao, G.-M. Jin, B.-G. Zhang, Z.-Y. Li, L.-M. Duan, H.-W. Wang, Z.-Y. Wei, Y.-Y. Li, S.-F. Wang, Z.-H. Lu, Y.-T. Zhu, H.-D. Zhu, and R.-J. Hu, Phys. Lett. B **538**, 39 (2002).
[34] L. G. Sobotka, M. A. McMahan, R. J. McDonald, C. Signarbieux, G. J. Wozniak, M. L. Padgett, J. H. Gu, Z. H. Liu, Z. Q. Yao, and L. G. Moretto, Phys. Rev. Lett. **53**, 2004 (1984).